URSI GASS 2023, Sapporo, Japan, 19 – 26 August 2023

Picosecond Non-Line-of-Sight Wireless Time and Frequency Synchronization for Coherent Distributed Aperture Antenna Arrays

Jason M. Merlo* and Jeffrey A. Nanzer
Electrical and Computer Engineering, Michigan State University, USA; e-mail: merlojas@msu.edu, nanzer@msu.edu

Abstract

Picosecond-level timing synchronization with wireless frequency transfer is presented in a non-line-of-sight (NLoS) environment using two software-defined radios (SDRs). Using a spectrally sparse pulsed two-tone waveform, high accuracy timing synchronization is achieved. Frequency synchronization is achieved via a continuous 10 MHz two-tone waveform transmitted between nodes which is demodulated by a self-mixing circuit to recover the 10 MHz reference signal used to discipline the local oscillator on the receiving SDR. Total time synchronization, beamforming, and phase accuracies of 8.84 ps, 23.17 ps, and 10°, respectively, were achieved enabling modulation bandwidths of up to 4.3 Gb/s at a carrier frequency of up to 1.33 GHz.

1 Introduction

Coherent distributed antenna arrays are rapidly gaining interest as an enabling technology for use in a large breadth of applications ranging from spaceborne adaptable high bandwidth sensing and communication systems [1, TX05.2.6] to cooperative automotive synthetic aperture imaging radars [2]. The motivation for coherent distributed aperture antennas derives from their ability to be reconfigured in deployment, robustness to single-node failure, and reduced mass and power density when compared with monolithic counterparts. Recently, efforts towards coherent distributed aperture arrays have been rapidly advancing demonstrating promising results in level of synchronization and coherent operations [3–6]. However, the majority of the focus has been on developing systems which work in line-of-sight (LoS) scenarios (with the exception of [6] which achieved ∼650 ns timing accuracy over a non-line-of-sight (NLoS) link), although ground-based distributed array applications may require operation in cluttered environments where LoS may not always be possible.

In this work we address the time and frequency synchronization aspects of distributed arrays in NLoS scenarios using a high accuracy pulsed two-tone time transfer technique and a two-tone continuous frequency transfer technique with the goal of picosecond-level synchronization. We evaluate the system-level temporal coherence by tracking the standard deviation of the system's time corrections and by measuring the temporal coherence of a secondary beamforming channel on each of the synchronized nodes at a centralized location connected via coaxial cables to evaluate expected beamforming performance.

2 Wireless Time-Frequency Synchronization

In distributed coherent arrays, it is essential that each of the nodes be aligned in time, frequency, and phase to ensure that coherent operations maximize the transmitted or received energy in the direction of interest [7]. The system time with a constant drift model on a node n within the array can be represented as

$$T_n(t) = \alpha_n t + \delta_n + \nu_n(t) \tag{1}$$

where t is the global true time, α_n is the rate of change of time at node n relative to the true time, δ_n is the initial time offset of node n, and $\nu_n(t)$ is zero-mean integrated timing error due to other system noise sources such as thermal, shot, and flicker noises [8, Ch. 10.1]. By applying a time synchronization technique, the initial time offset and slowly varying integrated errors can be mitigated, and then by frequency synchronizing, or *syntonizing*, the nodes, α_n can be made equal across all nodes.

The high-accuracy two-way time transfer (TWTT) process used for timing synchronization in this paper is described in detail in [5]. The process relies on estimating the time offset between nodes by sending a pair of timestamped messages between two nodes in a two-way exchange, marking the transmit and receive time of each message at each node. Assuming the channel is quasi-static and reciprocal during the synchronization epoch, the time offset between nodes m and n can be estimated by differencing the apparent time of flight (ToF) on each:

$$\Delta_{mn} = \frac{(t_{\mathrm{RX}m} - t_{\mathrm{TX}n}) - (t_{\mathrm{RX}n} - t_{\mathrm{TX}m})}{2} \tag{2}$$

where $t_{\mathrm{TX}n}$, $t_{\mathrm{RX}n}$ are the times of transmit and receive at the nth node, respectively. Once estimated, this offset can be added to the local clock at node n to compensate for the offset. In a similar way, the internode propagation delay τ_{mn} may be estimated by taking the average ToF between systems. However, Δ_{mn} and τ_{mn} are only as accurate as the individual time delay estimates themselves. To achieve

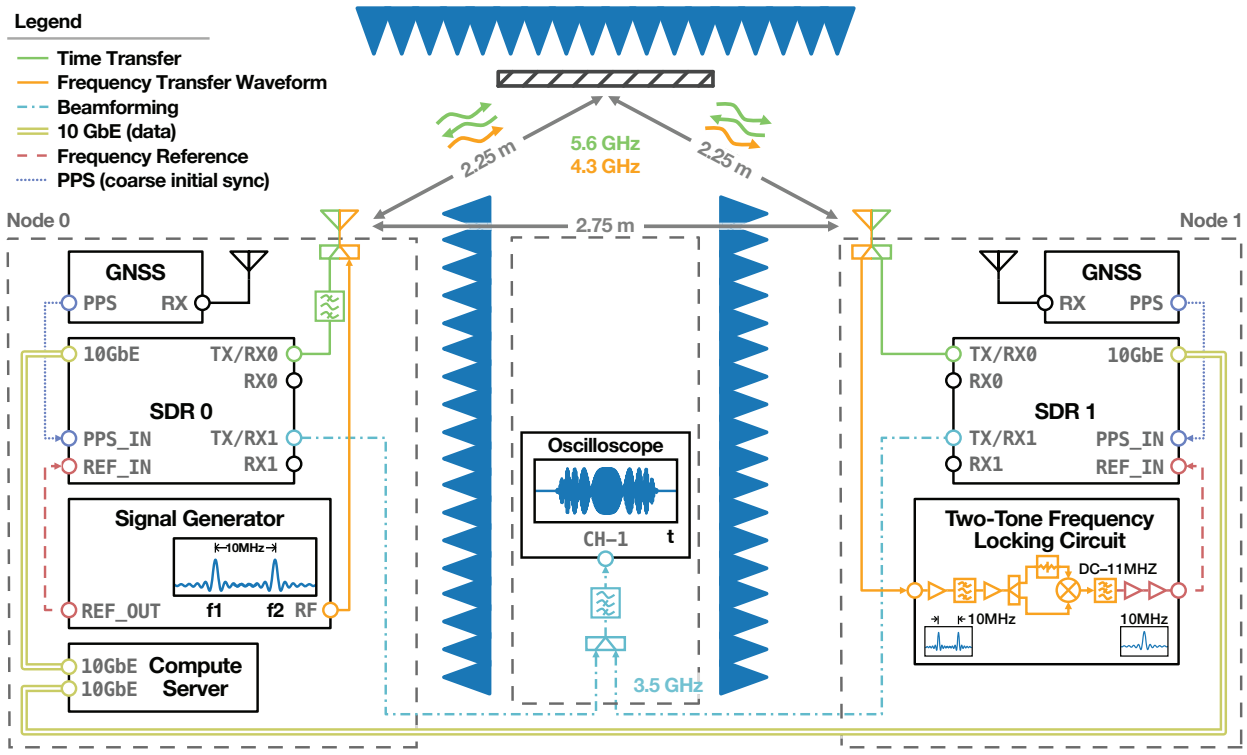

Figure 1. System schematic. Node 0 acted as the primary node generating the 10 MHz frequency reference for software-defined radio (SDR) 0 and the two-tone frequency transfer waveform for software-defined radio (SDR) 1. Global navigation satellite system (GNSS) receivers were used on each node to generate a pulse-per-second (PPS) signal for coarse initial timing synchronization. The time and frequency transfer waveforms were transmitted off a reflecting metal sheet and line-of-sight (LoS) was obstructed between the nodes by RF absorber, shown as blue triangles. To evaluate potential beamforming performance, the secondary channel on each software-defined radio (SDR) transmitted orthogonal linear frequency modulation (LFM) waveforms to an oscilloscope.

a high level of accuracy in arrival time estimation a two-tone waveform is chosen which minimizes the Cramer-Rao lower bound for time delay estimation [9]. While the absolute time delay of the two-tone waveform may be ambiguous in the presence of multiple scatterers, if the above assumptions on reciprocity and quasi-stasis are met, the time delay estimation, and thus timing synchronization, will be unaffected. For NLoS scenarios the signal-to-noise ratio (SNR) will likely degrade compared with a direct path, resulting in an accuracy loss following the theoretical bound.

To perform the time delay estimation, a matched filter is implemented in the Fourier domain as $s_{\mathrm{mf}}(t) = \mathscr{F}^{-1}\left(S_{\mathrm{RX}} S_{\mathrm{TX}}^{*}\right)$ where the signal is zero-padded prior to the inverse Fourier transform to improve ambiguity resolution of sidelobes which are similar in height during the refinement process [10, Ch. 4.2]. In this work a factor of 3 was used for interpolation. Next, the time delay was estimated by fitting a parabola to the peak of the matched filter using quadratic least-squares (QLS) [10, Ch. 7.2]; the peak value of a parabola can be solved for directly in closed form, providing an efficient means of delay estimation refinement of the matched filter to below a sample period, without significant interpolation. Finally, though the QLS efficiently refines the estimate to a small fraction of the sample period, a small residual error remains due to a mismatch between the true shape of the matched filter peak, and that of a parabola. This, however, is a function of the transmitted waveform, which is known a priori, and a lookup table may be used to compensate for this in realtime, reducing residual bias to negligible levels [5].

For frequency syntonization this work implemented a continuous-wave two-tone frequency transfer system, described in detail in [11], which utilizes a self-mixing receiver to generate a reference frequency, shown schematically in the lower-right corner of Figure 1. The system transmits a two-tone waveform with a tone spacing proportional to the frequency reference of the system of interest—in this work 10 MHz—which is filtered and downconverted by mixing the received signal with itself, and then low-pass filtered to remove higher frequency components resulting in a frequency at the output which is proportional to the two-tone spacing. Because this system uses a continuous wave frequency, the effect of propagation in a complex environment will be the sum of multiple phase-delayed copies of the two-tone waveform. In certain cases, this may cause destructive interference if the multi-path scatters add incoherently, however the frequency remains unperturbed, and thus tolerant to static NLoS where multipath may significantly affect the received signal.

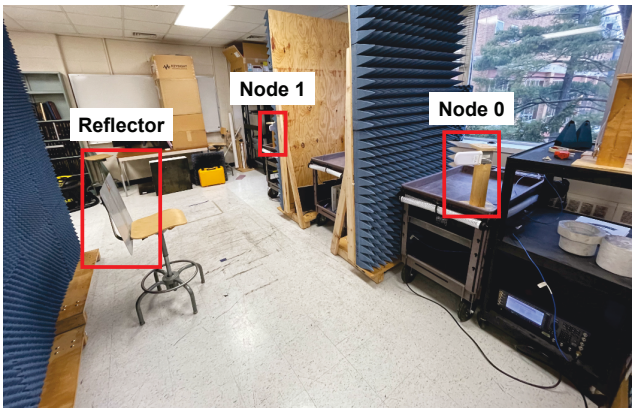

Figure 2. Experimental setup. Node 0 and the reference signal generator used for frequency transfer are shown at the right, the oscilloscope used to measure beamforming performance is on the cart between the blue RF absorber walls, and the cart for Node 1 is shown behind the far absorber wall. A chair with a metal sheet was used as a reflecting target for the time-frequency transfer signal shown on the left, backed by another absorbing wall.

3 System Configuration

A schematic of the time-frequency transfer system and a photograph of the experimental setup and testing environment can be found in Figures 1 and 2 respectively. The system utilized in this experiment consisted of two Ettus Research X310 software-defined radios (SDRs) running at 200 MSa/s, each containing two UBX-160 daughterboards with 160 MHz of instantaneous RF bandwidth. The SDRs were controlled via GNU Radio 3.10 and Ettus Universal Software Radio Peripheral Hardware Driver 4.4.0.0 on Ubuntu 22.04. Each node was separated by a wall of wideband RF absorber to obscure line-of-sight (LoS). Both the time and frequency transfer waveforms were power combined/split using a Mini-Circuits ZX10-2-852-S+ 0.5–8.5 GHz power combiner and transmitted/received on each node using two identical L-Com HG2458-08LP 8-dBi Log-Periodic antennas, steered to reflect the signal off a flat metal sheet between the two nodes.

To achieve a consistent 200 MSa/s, the devices were configured for burst operation which would transmit and receive short bursts of information to ensure the host server would avoid any streaming over/underflows. However, to ensure that the 30 µs transmit and receive windows shared enough overlap to successfully begin the high-accuracy time transfer process, global navigation satellite system (GNSS) receivers were used to first coarsely align the clocks on each SDR; this would time synchronize the system to ∼10 ns after which the high-accuracy time transfer process is used to refine the timing offsets to the picosecond level. The time transfer waveforms used had a 50 MHz tone separation and were transmitted at a carrier frequency of 5.6 GHz with a pulse duration of 10 µs. To achieve wireless frequency transfer, a Keysight E8267D Vector Signal Generator was used to generate a continuous 10 MHz two-tone signal which was transmitted with at a center frequency of 4.3 GHz at a power level of +21 dBm. A Mini-Circuits VHF-5050+ 5.5–10.0 GHz high-pass filter was used on node 0 to mitigate out of band interference from the continuous frequency transfer transmitter on the received time transfer signal. On node 1, the continuous 10 MHz two-tone frequency transfer signal was demodulated using the two-tone self-mixing circuit described in Sec. 2 which provided a 10 MHz reference signal for SDR 1. The experiment was run both with wireless frequency transfer and without to assess the impact of the frequency transfer on time synchronization and beamforming stability.

To evaluate the beamforming performance potential of the system, the second daughterboard on each SDR was connected to a Keysight DSOS804A 20 GSa/s oscilloscope via a ZX10-2-852-S+ power combiner; a Mini-Circuits VHF-3100+ 3.4–9.9 GHz high-pass filter was used to remove low-frequency switching transients from the start- and end-of-burst on the daughterboards. Each SDR transmitted orthogonal 100 MHz linear frequency modulation (LFM) waveforms (one up-chirp, one down-chirp), which were digitized on the oscilloscope and matched filtered against to determine the relative inter-arrival time and phase offsets from each node.

4 Non-line-of-sight Time-Frequency Transfer Experiment

In the time-frequency experiments, the time transfer signal transmit and receive gains were varied to achieve a SNR range of 6–30 dB to determine the impact of SNR on the time transfer stability. The experiments were repeated in two configurations: one with a physical coaxial cable linking the frequency reference inputs on each SDR, and with the two-tone wireless frequency transfer system to assess the impact of using wireless frequency transfer on the overall system time and beamforming stabilities. Each standard deviation value was computed using ∼1 min of samples, or between 30–40 measurements. During the experiment the TWTT exchange process occurred directly before the beamforming to ensure the beamforming operation occurred at the moment of maximum temporal coherence. A delay of ∼1.5 s occurred after the beamforming pulses to perform the LFM matched filtering and write the data to disk, limiting the overall system resynchronization rate.

The standard deviation measurements of the system time synchronization and beamforming internode arrival are shown in Figures 3a and 3b for the wired and wireless frequency transfer experimental configurations, respectively. In the wired frequency transfer configuration, the system time and beamforming interarrival time standard deviation reached levels of 5.93 ps and 17.67 ps, respectively, with a beamforming phase stability of 0.67° at 3.5 GHz. This corresponds with a maximum information bandwidth

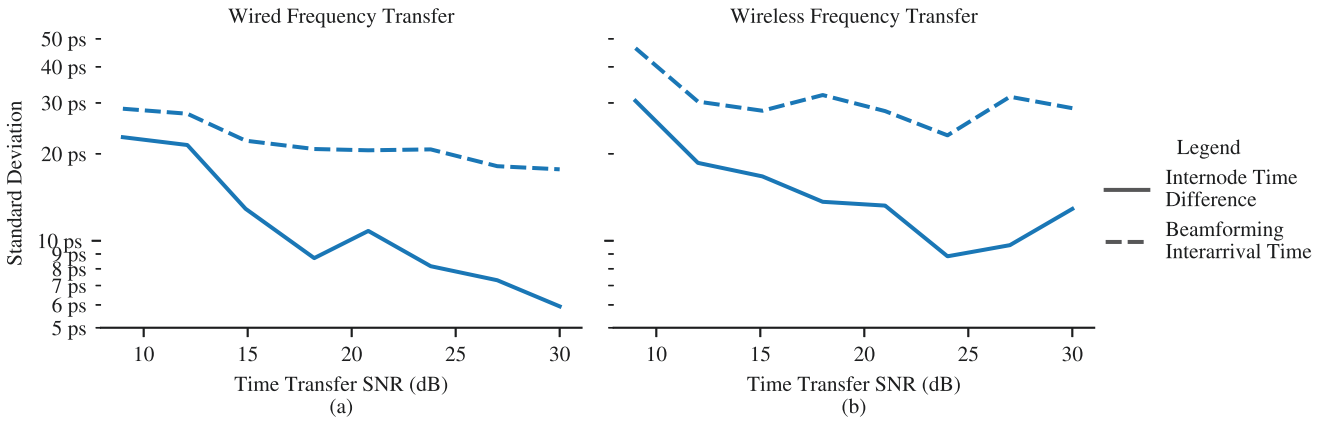

Figure 3. Internode time transfer synchronization and beamforming pulse interarrival time accuracy for the (a) wired and (b) wireless frequency transfer configurations.

of 5.6 Gb/s, assuming a binary encoding scheme such as amplitude-shift-keying (ASK) or binary phase-shift keying (BPSK) at up to 19 GHz [7, 12]. The wireless frequency transfer configuration achieved system time and beamforming interarrival time standard deviations of 8.84 ps and 23.17 ps respectively, with a beamforming phase stability of 10°. This corresponds with a maximum beamforming information bandwidth of 4.3 Gb/s at a carrier frequency of up to 1.33 GHz.

5 Conclusion

In this work it was demonstrated that the use of a high-accuracy spectrally sparse pulsed two-tone TWTT technique in coordination with a continuous two-tone frequency transfer technique is sufficient for NLoS time-frequency synchronization with multigigabit beamforming information bandwidths at carriers of over 1 GHz in a static environment. This verifies the operability of distributed arrays using these techniques for longer range operation where LoS may be intermittent or not possible, while still achieving high performance of coherent operations.

References

[1] "2020 NASA technology taxonomy," National Aeronautics and Space Administration, Tech. Rep. HQ-E-DAA-TN76545, Jan. 2020.

[2] D. Tagliaferri, M. Rizzi, S. Tebaldini, M. Nicoli, I. Russo, C. Mazzucco, A. V. Monti-Guarnieri, C. M. Prati, and U. Spagnolini, "Cooperative synthetic aperture radar in an urban connected car scenario," in *2021 1st IEEE International Online Symposium on Joint Communications & Sensing (JC&S)*. IEEE, 2021, pp. 1–4.

[3] S. Prager, M. S. Haynes, and M. Moghaddam, "Wireless subnanosecond RF synchronization for distributed ultrawideband software-defined radar networks," *IEEE Trans. Microw. Theory Techn.*, vol. 68, no. 11, pp. 4787–4804, 2020.

[4] J. E. Gilligan, E. M. Konitzer, E. Siman-Tov, J. W. Zobel, and E. J. Adles, "White rabbit time and frequency transfer over wireless millimeter-wave carriers," *IEEE transactions on ultrasonics, ferroelectrics, and frequency control*, vol. 67, no. 9, pp. 1946–1952, 2020.

[5] J. M. Merlo and J. A. Nanzer, "Wireless picosecond time synchronization for distributed antenna arrays," *IEEE Trans. Microw. Theory Techn.*, 2022.

[6] O. Seijo, J. A. López-Fernández, H.-P. Bernhard, and I. Val, "Enhanced timestamping method for subnanosecond time synchronization in IEEE 802.11 over WLAN standard conditions," *IEEE Trans. Ind. Informat.*, vol. 16, no. 9, pp. 5792–5805, 2020.

[7] J. A. Nanzer, R. L. Schmid, T. M. Comberiate, and J. E. Hodkin, "Open-loop coherent distributed arrays," *IEEE Trans. Microw. Theory Techn.*, vol. 65, no. 5, pp. 1662–1672, 2017.

[8] D. Pozar, *Microwave Engineering*, 3rd ed. John Wiley & Sons, Inc., 2005.

[9] J. A. Nanzer and M. D. Sharp, "On the estimation of angle rate in radar," *IEEE Trans. Antennas Propag.*, vol. 65, no. 3, pp. 1339–1348, 2017.

[10] M. Richards, *Fundamentals of Radar Signal Processing, Second Edition*. McGraw-Hill Education, 2014.

[11] S. R. Mghabghab and J. A. Nanzer, "Open-loop distributed beamforming using wireless frequency synchronization," *IEEE Trans. Microw. Theory Techn.*, vol. 69, no. 1, pp. 896–905, 2021.

[12] J. A. Nanzer, S. R. Mghabghab, S. M. Ellison, and A. Schlegel, "Distributed phased arrays: Challenges and recent advances," *IEEE Trans. Microw. Theory Techn.*, vol. 69, no. 11, pp. 4893–4907, 2021.